19th Australasian Fluid Mechanics Conference
Melbourne, Australia
8-11 December 2014

Cleaning of Viscous Droplets on an Inclined Planar Surface Using Film Flows

J.R. Landel[1], A.L. Thomas[2], H. McEvoy[3] and S.B. Dalziel[1]

[1]Department of Applied Mathematics and Theoretical Physics
University of Cambridge, Cambridge, Cambridgeshire, CB3 0WA, United Kingdom

[2]Department of Physical and Environmental Sciences
National University of Central Buenos Aires, Tandil, Buenos Aires Province, Argentina

[3]Defence Science and Technology Laboratory
Salisbury, Wiltshire, SP4 0JQ, United Kingdom

Abstract

We investigate the fluid mechanics of cleaning viscous drops attached to a flat inclined surface using thin gravity-driven film flows. We focus on the case where the drop cannot be detached from the surface by the mechanical forces exerted by the cleaning fluid on the drop surface. The fluid in the drop dissolves into the cleaning film flow, which then transports it away. We present a mathematical model for the mass transfer of the viscous fluid from the droplet into the film flow. The model assumes that the droplet has a negligible impact on the film velocity. To assess the impact of the drop on the velocity of the cleaning fluid, we have developed a novel experimental technique based on particle image velocimetry. We find that at intermediate Reynolds number the streamwise velocity can be strongly affected by the presence of the droplet. We discuss this impact on the cleaning of the droplet. Using the dye attenuation technique, we also measure the convective mass transfer of some dye mixed into the droplet and diffusing into the falling film. We find that the total amount of dye in the droplet decreases exponentially in time.

Introduction

Cleaning of fouling deposits using film flows is a common problem in many industrial processes, particularly in the food industry (*e.g.* Wilson [7]). The shearing action of a film flow is often used to clean fouled surfaces in industrial processes as well as in our daily life (Yeckel and Middleman, [8]), such as in a household dishwasher. In a full dishwasher, a jet of water impinges on the surface of some of the plates while others are simply covered by a thin draining film. The ability of the film to clean the drops of grease attached onto the plate surface is critical. Moreover, minimizing the water consumption and the energy of such automatic cleaning devices can have an important environmental and sustainable impact. In this study, we investigate the case where shear forces cannot overcome adherence, and thus the drop remains attached onto the surface until it dissolves completely in the film. The drop can deform, elongate and slide over the substrate at a rate which is negligible compared with the typical advection rate.

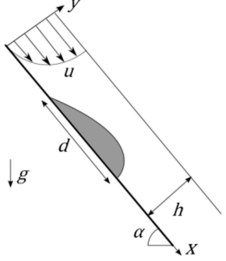

Figure 1. Schematic diagram of the cleaning problem. A liquid film flows over a viscous drop (shaded).

We are interested in the case of cleaning a single drop of viscous liquid lying on an inclined planar surface using a gravity-driven falling film (see figure 1). Blount [1] developed a mathematical model for the dissolution and transport of the fluid from the drop into the film flow. The streamwise velocity in the film is obtained assuming a viscous–gravity balance and the lubrication approximation,

$$u_\infty(y) = \frac{g \sin\alpha}{2\nu} y(2h_\infty - y), \qquad (1)$$

where y is the spatial coordinate in the direction orthogonal to the substrate (x the streamwise direction and z the lateral or spanwise direction), g is the constant of gravity, α is the inclination angle of the substrate from horizontal, ν is the film kinematic viscosity and h_∞ is the far-field film thickness. The drop fluid (shaded in figure 1), considered as a passive tracer, is described using the advection–diffusion equation in the film phase

$$\partial_t A + \boldsymbol{u} \cdot \boldsymbol{\nabla} A = D\nabla^2 A, \qquad (2)$$

where ∂_t is the partial differentiation with respect to time, A is the local concentration of the drop fluid, $\boldsymbol{u} = (u, v, w)$ is the local film velocity and D is the constant diffusion coefficient of the drop fluid in the film phase. Assuming that just outside the drop interface A is fixed, and equal to the maximum solubility, A_s, of the drop fluid in the film phase, and that the film fluid forms a momentum boundary layer such that $u \propto y$, [1] solved equation (2) to obtain a prediction for the total flux of drop fluid, integrated along the drop surface, into the film flow

$$F = 0.808 A_s \left(\frac{3g^2 D^6 \Gamma d^6 \sin^2\alpha}{\nu^2}\right)^{1/9}, \qquad (3)$$

where Γ is the two-dimensional flow rate and d is the drop length.

Our objective is to test the validity of the model developed by [1], particularly some of the assumptions made to derive the flux F, using some experimental measurements. [1] makes two important assumptions in his model. Firstly, he assumes that the film velocity is not affected by the drop; secondly, that the flux F does not depend on time and can be found by solving the advection–diffusion equation (2) at steady state. For simplicity, we focus here on the case of a non-deformable drop, which corresponds to the very viscous limit. We test the first assumption by measuring the velocity field of the film flow in the vicinity of a solid obstacle, representing a non-deformable drop (Landel *et al.* [5]). To assess the second assumption, we perform some dye attenuation experiments to measure the characteristic time scale of the mass transfer between a very viscous non-Newtonian droplet and the flowing liquid film.

Experimental Procedures

Measuring the Film Velocity Field in the Vicinity of the Drop

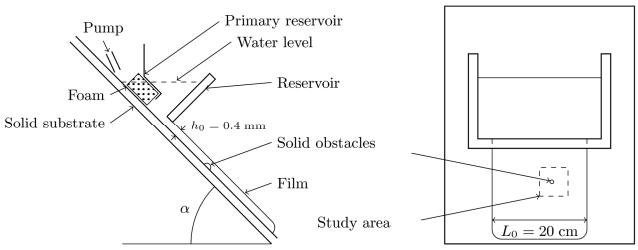

Figure 2. Schematic diagram of the experimental apparatus. Left: side view; right: top view.

We produced gravity-driven thin film flows in the experimental apparatus shown schematically in figure 2 (see [5] for more details). A liquid film flowed from a constant-head reservoir through a thin gap on a flat solid substrate inclined at an angle α to the horizontal. The film flowed freely over a one millimetre thick sheet of polished stainless steel. The stainless steel substrate was cleaned before each experiment with some water and soap, vinegar-based de-scaler and finally isopropanol. The film flowed on the substrate for a distance of approximately 300 mm from the outlet of the reservoir gap to the bottom-end of the substrate, and then fell freely into a large collecting tank. The flow rate of the film was maintained constant. The fluid could recirculate in the experimental apparatus using a submersible pump located in the collecting tank. The fluid was pumped into a primary reservoir located upstream of the main reservoir. The fluid turbulence in the primary reservoir was dampened as it penetrated through a piece of foam and a 5 mm gap into the main U-shaped reservoir. Once the flow was stable, we recorded the experiment with a high-speed grey-scale camera, Photron–Fastcam SA1.1, mounted with a 60 mm focal-length lens and a UV/IR blocking filter. We filtered out the infrared part of the spectrum because the camera was sensitive to this part of the spectrum. Two 300 Watts arc lamps and two 250 Watts halogen lamps produced a uniform illumination on the film with minimal shadows or reflections at the crests and troughs of surface waves.

Exp.	Angle (°)	Q (cm^3 s^{-1})	Resolution (pixel)	View (cm^2)
1	44	50	1024×1024	17×17
2	44	50	1024×896	3.4×3.0

Exp.	Frame Rate (Hz)	Shutter time (s)	$\mathrm{Re} = 4\Gamma/\nu$
1	2000	1/3000	1000–1200
2	6250	1/9000	1100

Table 1. Summary of the control parameters for all the experiments.

The details of the control parameters for the two experiments shown in this paper are presented in table 1. For Exp. 1, the camera view is centred on the film mid-width and with the top of the image just above the outlet, so as to see the film immediately after flowing through the gap. We analysed the images using *DigiFlow* (Dalziel *et al*. [3]). The spatial velocity resolution is 2.7 mm. The film Reynolds number is defined as $\mathrm{Re} = 4\Gamma/\nu$ with $\Gamma(x) = Q/L(x)$, Q the three-dimensional constant flow rate, and L the local film width along the spanwise direction. In Exp. 1, the camera view is centred on the obstacle in the flow. The resolution is approximately four times larger so that we have a very detailed measurement of the flow in the vicinity of the obstacle. The new spatial velocity resolution is 0.7 mm.

The film liquid used for the PIV experiments was a mixture of 4 litres of cold water with approximately 40 g of methylene blue and 20 g of artificial pearlescence, which was made of titanium-dioxide coated mica particles (Iriodin 120 pigment, Merck; size: 5 to 25 microns; density: 3 g cm^{-3}). The purpose of this very dark mixture of dye was to render the film opaque for the camera so that only the surface of the film could be seen. The artificial pearlescence comprised small plates acting as tracers, aligning with the shear. These tracers produced a non-uniform reflecting texture of light intensity at the surface of the film, from which the surface velocity could be computed using a PIV algorithm in *Digiflow*.

The impact of a solid obstacle on the film flow was studied. We made a small obstacle by sticking a piece of Blu-Tack (Bostik) on the substrate located at a distance of approximately 91 mm downstream of the outlet and approximately 10 mm to the right of the centreline. The size of the obstacle was 0.5 to 0.8 mm in thickness and 2.8 mm in diameter. The shape was a rough flattened hemisphere, which modelled the shape of a very viscous sessile drop. According to the results obtained using different obstacles (including perfect spherical metal beads in a slightly different setup), we believe that the small imperfections of our hand-shaped obstacles had a limited impact on our measurements of the surface velocity field. The film flow was fully developed at the location of the obstacle. The obstacle was fully submerged by the film.

Measuring the Mass Transfer from the Drop into the Film

We measured the temporal evolution of the concentration of methylene blue in a polymer-thickened droplet submerged in a thin falling film. The droplets contained a non-ionic water-soluble polymer Natrosol 250 hydroxyethylcellulose (HEC) produced by Aqualon. We mixed the 250HHR-type polymer with tap water at a concentration of 2% wt. We performed the measurements in the experimental setup described in figure 2. One or more drops were aligned (sufficiently far apart to neglect the influence on neighbouring drops) on the substrate at a distance of approximately 8 to 10 cm away from the source reservoir, where the flow was fully developed. The substrate we used in these experiments is glass. We measured the total dye concentration remaining in the droplet using the dye attenuation technique. We used a Jai camera (CVM4+CL) mounted with a 75 mm lens. We performed the experiments in a dark room. We used an array of 6 × 9 red LEDs (TruOpto) in combination with a diffusive white acrylic sheet to produce a constant, uniform light source. This light source was located 20 cm behind the back of the glass substrate. The peak wave length of the LEDs, 625 nm, was close to the absorption peak wave length of methylene blue: 664 nm. We measured the transmitted light intensity with the camera described above. The camera was located approximately 0.5 m away from the substrate, which was sufficient to neglect parallax error. The frequency of image acquisition was set at 24 frames per second for a duration of a few minutes, until the droplet appeared clear to the dye detection setup. We followed the calibration method and the algorithm described by Cenedese and Dalziel [2]. We performed all the calibrations in situ. All the images recorded by the camera are analysed using *DigiFlow*. We obtained a relationship between the intensity recorded by the camera and the depth-averaged concentration in the liquid flowing on the surface at the location of the drop.

We conducted 7 experiments for a total number of 59 drops for different initial drop volumes $0.5 \leq V_0 \leq 4.5$ cm^3, different substrate angles $20 \leq \alpha \leq 45°$, different flow rates $46 \leq Q \leq 96$ cm^3 s^{-1}, and different film thicknesses $0.4 \leq h_\infty \leq 1.0$ mm. The film Reynolds number ranged from 2200 to 4500. The initial concentration of methylene blue was fixed for all the experiments at the same value: $C_{MB} = 0.02\%$ wt.

Experimental Results

Film Velocity Field in the Vicinity of the Drop

In figure 3, we present the distribution of the local time-averaged surface velocity $\bar{u}$ of the film and its standard deviation (dashed curves) along the streamwise (x) direction. The velocity is non-dimensionalised by the depth-averaged velocity as $x \to +\infty$, i.e. $< u_\infty >$ computed from equation (1). We plot with crosses the velocity distribution taken at a lateral location where the flow is disturbed by an obstacle, which is located within the two dashed vertical lines. The profile plotted at the location of the obstacle (crosses) shows a clear and strong disturbance of the time-averaged surface velocity both upstream and downstream of the obstacle. The disturbance propagates approximately one obstacle diameter upstream. At $4x/(h_\infty \mathrm{Re}) \approx 0.6$ we can note first a very small decrease of the velocity followed by a slight increase. Then the velocity drops sharply over the obstacle, by approximately 20 to 50%, compared with the undisturbed velocity (plotted with pluses), which asymptotes towards the predicted undisturbed far-field value.

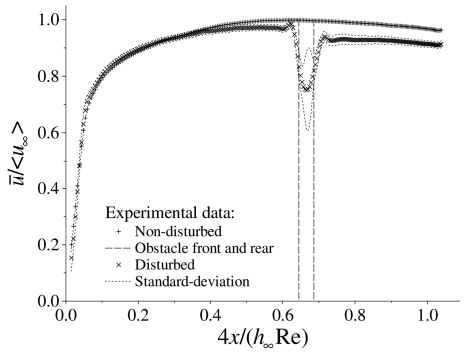

Figure 3. Non-dimensional distribution of the time-averaged surface velocity of the film (crosses) and its standard deviation (dotted curves) along the streamwise (x) direction at a lateral (z) location where the flow is disturbed by an obstacle (located between the two dashed vertical lines). The non-disturbed data are plotted with pluses for comparison.

The decrease is found consistently throughout the different experiments. The velocity increases again after the flow passes the centre of the obstacle. However, we can see that in the wake of the obstacle the surface velocity remains 5% lower than the undisturbed velocity. Comparing the different experiments, the velocity recovers its undisturbed value after 5 or more obstacle diameters downstream. The recovery distance tends to increase with Reynolds number. The profile of the disturbed surface velocity presented is typical across all the experiments we conducted. Only the magnitude of the velocity reduction and the recovery distance vary between the experiments. We believe that the velocity reduction is strongly related to the film thickness at the obstacle, which could not be measured in our experiment but was estimated between 0.1 and 0.3 mm. The far-field undisturbed film thickness varies from 0.4 and 1 mm in our experiments.

In figure 4, we show the spatial distribution of the surface velocity for the non-dimensional time-averaged streamwise velocity $\bar{u}/< u_\infty >$ (figure 4a), and the non-dimensional time-averaged lateral velocity $\bar{w}/< u_\infty >$ (figure 4b). The obstacle is located at $(x, z) = (x_0, 0)$ on the right-hand-side and top axis. Upstream of the obstacle, we can see that the amplitude of the time-averaged surface velocities $\bar{u}$ and $\bar{w}$ are fairly uniform. In figure 4(a), we can see that the impact of the obstacle on the streamwise velocity is very limited upstream, but spreads laterally due to the formation of stationary capillary waves. These capillary waves, or 'bow waves', have a characteristic V shape similar to the wave front in the wake of ships (Pozrikidis and Thoroddsen, [6]; Gaskell *et al.* [4]). As we observed in figure 3, the magnitude of the velocity does not recover its upstream value in the wake of the obstacle, for a band ranging the full width of the obstacle.

In figure 4(b), we should first note that the magnitude of the lateral velocity is at most 3% of the magnitude of the undisturbed streamwise velocity. The diverging flow on the obstacle is clearly visible in the velocity field, starting exactly at the top edge of the obstacle. Then, immediately downstream of the obstacle, $\bar{w}$ points inwards revealing flow convergence in a narrow region extending more than five obstacle diameters downstream. At the bottom edge of the obstacle, the flow is quite complex and three-dimensional. We find that the standard deviation is rather large in this region. It is possible that the tracers segregate away from this region owing to the divergence of the flow immediately upstream. The V-shape pattern of the stationary capillary waves is also clearly revealed by the distribution of the lateral velocity.

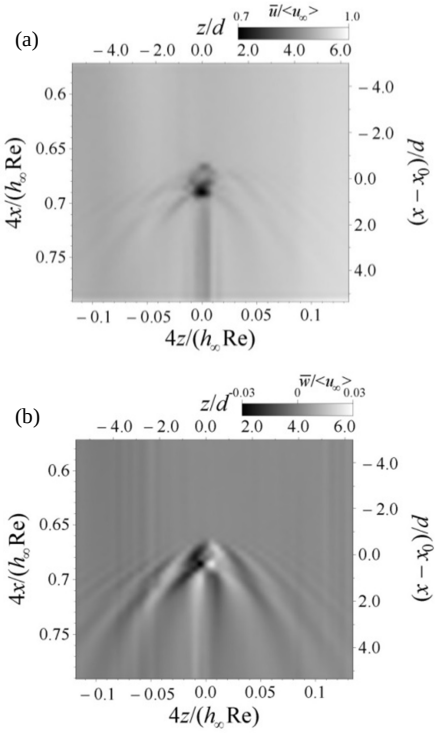

Figure 4. Spatial distribution of the surface velocity of a film flowing over a fully submerged obstacle (located at $(x, z) = (x_0, 0)$ on the right-hand-side and top axis) at an angle of 44°, a flow rate of 50 cm^3 s^{-1} (Exp. 5 in Table 1). (a) Non-dimensional time-averaged streamwise velocity; (b) non-dimensional time-averaged lateral velocity (with negative values, in darker grey, pointing to the left).

Mass Transfer from the Drop into the Film

In figure 5, we plot the concentration of methylene blue (normalised with the initial concentration $C_{MB,0}$) as a function of non-dimensional time $t\,\kappa/(V_0/A(t))$ (where κ is the mass transfer coefficient and A is the area of the interface between the droplet and the film) for the ensemble average of the data in each experiment (plotted with pluses of different colours). Best least-squares exponential fits (with κ as fitting parameter) are plotted with solid lines of similar colour as the data following

$$\frac{C_{MB}}{C_{MB,0}} \approx \exp\left[-\frac{\kappa A}{V_0} t\right]. \qquad (4)$$

The experimental data are corrected for the non-linear detection issue with the dye and camera system, occurring where the depth-integrated concentration of dye is lower than the detection threshold. We make the assumption that the time-dependent drop shape can be approximated by a spherical cap of constant volume, but time-dependent shape. By further assuming that the concentration is approximately uniform throughout the droplet,

we can estimate the quantity of dye invisible to the camera. We can observe that all the experimental data decrease exponentially at roughly the same rate, irrespective of drop size, Reynolds number, film thickness, substrate angle, or flow rate. In particular, we find that the time to reduce the concentration of dye in the droplet to 10% of its initial quantity is approximately $t_{10\%}\kappa/(V_0/A) = 2.3$.

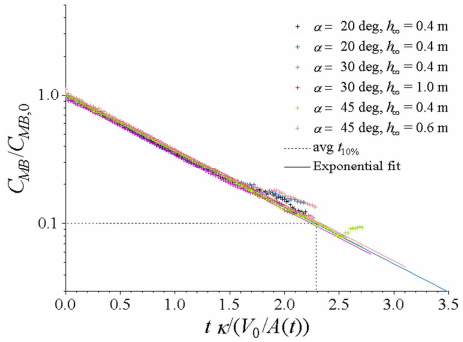

Figure 5. Normalised concentration of methylene blue dye (C_{MB}) in the drop versus non-dimensional time. We plot the ensemble averaged data for each experiment with pluses of different colours and the corresponding exponential fits with solid lines.

In his model, [1] considered only the steady state of the advection–diffusion equation (2) to derive the expression of the flux (3). According to our experimental results presented in figure 5, we find that the characteristic time scale of the mass transfer is $\tau_\kappa = V_0/(\kappa A) \approx 10$ to 100 s, whereas the time scale for the establishment of the diffusive boundary layer is much smaller: of the order $\tau_D = 10^{-1}$ s ([1]). Therefore, we have found an experimental validation for Blount's hypothesis that the convective flux of dye out of the droplet is in quasi-steady state.

Conclusions

We have investigated the problem of cleaning a very viscous drop attached to an inclined surface by a gravity-driven falling film flowing over the drop. We are interested in the case where the film cannot detach the drop from the substrate. Instead, the drop fluid diffuses slowly into the cleaning film before being transported away by the bulk flow. This problem was modelled theoretically by [1] using an advection–diffusion equation. We have tested experimentally two of the key assumptions in the model: first, that the drop does not impact the velocity in the diffusive boundary layer at the interface; second, that the flux for the mass transfer does not depend on the evolution in time of the concentration inside the droplet.

To test [1]'s first assumption, we have developed a new experimental technique, based on particle image velocimetry, to measure the velocity field at the surface of a liquid film. We report in this study the first measurements of the two-dimensional distribution of the film surface velocity in the vicinity of an obstacle. The film Reynolds number was in the intermediate range: 1000–1200. When undisturbed, we observed that the surface velocity of the film reached asymptotically the viscous–gravity regime. On the other hand, an obstacle submerged in the film had a strong impact on the film velocity. We noted a large decrease in the magnitude of the streamwise velocity starting one obstacle diameter upstream of the obstacle. The recovery of the streamwise velocity downstream of the obstacle could be larger than 10 obstacle diameters. Laterally, characteristic V-shaped capillary waves perturbed the velocity field. The magnitude of the disturbance due to the waves was small compared with the disturbance at the obstacle. We could also observe a complex three-dimensional converging flow just below the obstacle. The reduction of the film velocity and the decrease of the film thickness in the vicinity of the obstacle can have an impact on the mass transfer between the drop and the film. If we assume that, similarly to the case of convective mass transfer in a Blasius boundary layer above a flat plate, the thickness of the diffusive boundary layer above the drop is related to the Schmidt number and the local Reynolds number such that $\delta_C \sim x\mathrm{Sc}^{-1/3}\mathrm{Re}_x^{-1/2}$, then we can note that δ_C increases with decreasing Reynolds number. Hence, the diffusive boundary layer thickness increases with decreasing velocity in the film: for instance, a decrease of 50% in the velocity corresponds to an increase of 40% in δ_C. Furthermore, increasing the diffusive boundary layer thickness tends to decrease the mass transfer at the interface, which means a lower cleaning rate of the droplets.

To test [1]'s second assumption, we measured the convective mass transfer of a dye tracer diffusing from the droplet into the submerging flowing film. We conducted many experiments varying the drop size, the film Reynolds number, the film thickness. We found that the concentration of dye inside the droplet decreased exponentially in time. We computed a characteristic time scale for the mass transfer which is much larger than the time scale for the establishment of the diffusive boundary layer above the interface. This result confirms the hypothesis of [1] that the flux can be computed considering only the steady-state advection–diffusion equation in the film flow.

In conclusion, the drop can affect the convective mass transfer into the film flow by decreasing significantly the velocity field in the film. The concentration of a species inside the droplet decreases exponentially in time, at a rate much slower than the establishment of the diffusive boundary layer developing in the film phase above the interface.

Acknowledgments

This material is based upon work supported by the Defense Threat Reduction Agency under Contract No. HDTRA1-12-D-0003-0001.

References

[1] Blount, M., Aspects of advection–diffusion–reaction flows of relevance to decontamination, *KTN Intern. Rep.*, 2010.

[2] Cenedese, C., & Dalziel, S.B., Concentration and depth field determined by the light transmitted through a dyed solution. *8th Int. Symp. Flow Vis.*, **61**, 1998, 1–5.

[3] Dalziel, S.B., Carr, M., Sveen, J.K. & Davies, P.A., Simultaneous synthetic schlieren and PIV measurements for internal solitary waves. *Meas. Sc. Tech.*, **18**, 2007, 533–547.

[4] Gaskell, P.H., Jimack, P.K., Sellier, M., Thompson, H.M. & Wilson, M.C.T., Gravity-driven flow of continuous thin liquid films on non-porous substrates with topography, *J. Fluid Mech.*, **509**, 2004, 253–280.

[5] Landel, J.R., McEvoy, H. & Dalziel, S.B., Cleaning of viscous drops on a flat inclined surface using gravity-driven film flows, in *Fouling & Cleaning in Food Processing 2014: Green Cleaning*, editors D.I. Wilson and Y.M.J. Chew, DCEB, University of Cambridge, 2014, 324–331.

[6] Pozrikidis, C., & Thoroddsen, S.T., The deformation of a liquid film flowing down an inclined plane wall over a small particle arrested on the wall, *Phys. Fluids A*, **3**, 1991, 2546–2558.

[7] Wilson, D.I., Challenges in cleaning: recent developments and future prospects, *Heat Trans. Eng.*, **26**, 2004, 51–59.

[8] Yeckel, A. & Middleman, S. Removal of a viscous film from a rigid plane surface by an impinging liquid jet, *Chem. Eng. Com.* **50**, 1987, 165–175.